Synthesis and Characterization of Manganese Ferrite nano-particles from Low-grade Manganese ore and Ferric oxide powder via Pyrometallurgy

Salar Ahmad
University of Peshawar
Sajjad Ali
University of Peshawar
Ikram Ullah
National University of Computer and Emerging Sciences Peshawar Campus
Sajjad ali
University of Peshawar
Wajaree Weera (wajawe@kku.ac.th)
khon kaen University

Article

Keywords: Synthesis, characterization, Sintering temperature, particle size, Ferric oxide and Mn-ore

Posted Date: July 1st, 2022

DOI: https://doi.org/10.21203/rs.3.rs-1773675/v1

Abstract

The present study focuses on the synthesis and characterization of manganese ferrite. Manganese ferrite has been synthesized by mixing ferric oxide powder (Fe_2O_3) with low grade Mn-ore and then sintering it at different temperatures (1000-1200 ^{0}C). the method is cheap, simple, and easily controls particle size. It has been established that manganese ferrite phase has been successfully achieved at all the three sintering temperatures however, a higher peak has been noted at sintering temperature of 1200 ^{0}C in XRD diffractogram. An increase in particle size with increasing sintering temperature has been reported. Thermal analysis shows a weight gain of ( ) at ( ) which further confirm the phase formation of manganese ferrite. Stretching vibrations were recorded at 1636 cm^{-1} while some peaks were observed below 1000 cm^{-1} in FTIR graph which is a common feature of ferrites. Microstructural analysis show small pores at the surface and confirm that the synthesized manganese ferrite nano-particles show best magnetic properties and possess high melting point. A highly synchronous nucleation and growth of the synthesized nanoparticles is also confirmed from TEM analysis. Overall, because of its simpleness and cheapness this method could be used for synthesis of manganese ferrite synthesis.

1. Experimental Procedure

In the present work, manganese ferrite is synthesized through pyrometallurgy. For manganese ferrite synthesis, the amount of Manganese and Iron was determined at an appropriate ratio i.e., Mn: Fe = 1:2. The samples were weighted via Weighting Balance (KERN ALS 220-4). For this purpose, low grade manganese ore powder (source of Mn) was mixed with of ferric oxide powder (Fe_2O_3) (source of Fe) for 1 hour in a pestle mortar system. After mixing, pellets (9mm) were made at a pressure of 1.7 mega Pascal using Manuel Pellet Press. Three batches were prepared, the batch-I, batch-II and batch-III pellets were heat treated at 1000, 1100 and 1200 ^{0}C for 7, 9 and 10 h respectively in high temperature furnace (Nabertherm- LHT04/18, Germany). Finally, the samples were forwarded for characterization.

X-ray study of the sample was attained via PANalytical X-ray diffractometer (XRD) with Cu Kα radiation (λ=1.5418 Å). X-ray study revealed that high intensity manganese ferrite phase along with large particle size is formed at a sintering temperature of 1200 ^{0}C while low intensity manganese ferrite phase appeared at sintering temperatures of 1000 and 1100 ^{0}C. therefore, the samples sintered at 1200 ^{0}C were forwarded for further characterization. Using Fourier transform infrared (FTIR) spectrometer (PerkinElmer, UATR Two), spectroscopic analysis of the sample was performed in which the levels of transmission are measured for wave numbers of 400-4000 cm^{-1}. Thermogravimetric analysis (TGA) of the sample was performed through thermogravimetric analyzer (**Pyris Diamond Series, Perkin Elmer, USA)** while differential scanning calorimetry (DSC) has been executed by using differential scanning calorimeter (**Diamond Series DSC, Perkin Elmer, USA). Microstructural analysis of the sample was carried out via (SEM) Scanning electron microscope (JSM5910 ,30kv, JEOL, Japan) and (TEM) tunneling electron microscope (JEM-2100, 200kv, JEOL, Japan)**. Elemental analysis of the sample was performed by EDX

(energy dispersive X-ray spectroscopy) and additionally, the sample was characterized via selected area electron diffraction (SAED).

2. Introduction

Manganese ferrite is a spinel ferrite and have an impact because of its greater surface to volume ratio [1]. Recently, ferrites (spinel) have been studied and probed due to its useful electric and magnetic properties and its use in, information storage systems, magnetic bulk cores, microwave absorbers, magnetic fluids, and medical diagnostics [2]. Researchers have much interest in synthesis and characterization of spinel ferrites specifically super paramagnetic metal oxide spinel ferrites [3, 4] and $MeFe_2O_4$ (metal Me = Co, Mg, Mn, Zn, etc.). Spinel ferrites have the general formula AB_2O_4, containing a somewhat perfect cubic closed packed oxygen alignment in which A and B are di-valent and tri-valent cations respectively. The cations lie at tetrahedral and octahedral interstices. Mn-ferrite is a partial inverse spinel ferrite in which the Mn^{+2} ions (20%) lies at B-sites means at the octahedral coordination sites and the remaining lies at the A sites means at tetrahedral coordination sites [5] as shown in figure 1. Previous studies reveal that the non- magnetic substitutions and magnetic ions migrate from one site to another site at high temperatures (> 900 0C) due to sufficient energy therefore, by conventional methods of synthesis the formation of spinel ferrites mostly takes place at temperatures greater than 900 ^{0}C [6].

Several synthesis techniques have been developed for obtaining manganese ferrite like co-precipitated hydroxides [7], oxalates [8], citrates [9], micelle and reverse micelle [10], in addition to combustion [11]. Manganese ferrite obtained through these processes is extremely pure, but these processes uses reactants of high cost and complex technological procedures. Sukmarani et al. [12] synthesized manganese ferrite from calcinated manganese ore and ferric oxide (Fe_2O_3) through mechanical milling and calcination and found that the formation temperature of Manganes ferrite falls due to the presence of milling process. Naseri et al. [13] synthesized manganese ferrite via thermal treatment followed by calcination and found that the sample's super-paramagnetic behaviour gets boosted as the calcination temperature rises. Yang et al. [14] synthesized manganese ferrite by solvothermal technique and investigated that the final samples possess high saturation magnetization along with porous structure. Pande et al. [15] prepared manganes ferrite nano particles using co-precipitation method by utilizing diethanolamine as precipitating and capping agent and found that the final samples have super paramagnetic properties and very large saturation magnetization, small coercivity and small remanence. Kafshgari et al. [16] synthesized manganese ferrite nanoparticles by hydrothermal route, co-precipitation, and sol-gel method and investigated lowest crystallite sizes for the samples which were synthesized through hydrothermal method. Zhang et al. [17] obtained manganese ferrite nanoparticles by co-precipitation technique and established that synthesis takes place without calcining.

All the techniques used for manganese ferrite synthesis were expensive, time lasting and complex. However, pyrometallurgy is regarded as economical, less time consuming and simple technological procedure in ferrite synthesis. Thus, manganese ferrite is mostly synthesized from very reactive and very

small grinded powders which are densified by through solid to solid reactions at very high sintering temperatures. Synthesis and characterization of Mn-ferrite from low grade Mn-ore through pyrometallurgy was the main goal of the present research work. In present work, the synthesis method in which low grade Mn-ore powder and Fe_2O_3 powder followed by sintering, has been adopted. This method of synthesis involve heating of the samples without melting and as a result the ores can be converted into oxides which may leave the in the form of gasses. Moreover, this technique is used for enormous production [18]. Finally, characterization of the synthesized Mn-ferrite is also presented in this paper.

3. Results And Discussion

3.1. X-ray (XRD) analysis

Figure 2(a, b, c) show diffraction patterns of the samples sintered at 1200, 1100 and 1000 ^{0}C respectively. The corresponding peaks are labelled as A, B, C and D. The high intensity peaks labelled as A show the formation of Mn-ferrite phase pdf# (74-2403). The peaks labelled as B, C and D represents the formation of MnO_2 (manganese oxide) phase pdf# (12-141), SiO_2 (silicon oxide) pdf# (28-476) and FeO (iron oxide) pdf# (46-1312) respectively. The reported (h k l) values for the peaks A, B, C and D are (1 1 1), (2 0 0), (2 2 0) and (3 1 1) respectively. These (h k l) values will be further studied in detail within SAED analysis.

Literature suggest that during the growth of nanoparticles, the micro strain developed in the nanoparticles can affect XRD peaks [20] therefore, it is very important to determine the crystallite size and micro strain of the synthesized manganese ferrite nanoparticles. The calculated values of average crystallite size D (nm) was determined with the help of Scherrer formula equation (1) and the average micro strain (□) calculated by using equation (2) along with respective temperatures are reported in table 1. A considerable increase in particle size has been observed from XRD analysis which is due to the increase in collisions probability at high temperatures and results in large number of movements of atoms. These larger number of movements of atoms further aid the arrangement of the crystalline structure [21]. A decrease in micro strain with increasing sintering temperature of the synthesized nanoparticles is also observed which show that the variations in lattice parameters of the synthesized nanoparticles considerably fall at high sintering temperatures. Table 1 reports positive micro strain values which show lattice expansion [20].

$$D = 0.89\lambda / \beta \cos\theta \quad (1)$$

Where D is the crystallite size, λ is wavelength of X-rays, β is the full width half maxima and θ is the corresponding angle of diffraction.

$$□ = \beta/4 \tan\theta \quad (2)$$

Where □ represent micro strain, β represent full width half maxima and θ is the corresponding angle of diffraction.

The dislocation density (δ nm^{-2}) calculated by using equation (3) is also depicted in table 1. A decreases in dislocation density is observed as the sintering temperature increases which show a decrease in ductility and a non-isotropic hardening of the synthesized nanoparticles. A detailed microstructural analysis will be presented in the upcoming sections.

$$\delta = 1/ D^2 \quad (3)$$

Where δ is dislocation density and D represents particle size.

Table 1

Showing change in particle size (D), micro strain (), and dislocation density (δ) with sintering Temperature

Sintering Temperature (^0C)	crystallite size D (nm)	Micro strain ($\times10^{-3}$)	Dislocation density δ$\times10^{-3}$ (nm^{-2})
1000	5.95	548.33	28.18
1100	6.37	155.58	24.63
1200	8.24	145.45	11.67

3.2. FTIR analysis

For the determination of chemical and structural changes, Fourier transform infra-red (FTIR) of the sample was performed. Figure (3) shows FTIR spectra of the synthesized sample. Many small peaks can be seen in the range 3600-1200 cm^{-1} labelled as region (a). The peak at 3421.7 cm^{-1} represents OH-group. C-H bending mode is confirmed by the peak appeared at 1093.44 cm^{-1} [22]. The asymmetric stretching vibration of O-C-O is attributed to the peak at 1636 cm^{-1} [23]. The peak at 471.18 cm^{-1} show stretching vibrations of intrinsic metal oxygen at octahedral sites while the peak at 552 cm^{-1} represents the stretching vibrations of metal oxides at the tetrahedral and octahedral positions [24]. Similar peaks were also observed by zipare et.al [25] hence the result is consistent with previously reported experimental results. Three major peaks were also observed below 1000 cm^{-1} i.e., at 786, 552 and 471.17 cm^{-1} in fig 3, which is a common feature of ferrites [25] thus FTIR analysis also confirmed the formation of ferrite nanoparticles (manganese ferrite).

3.3. Thermogravimetric (TGA) and differential scanning calorimetry (DSC) analysis

The study of weight loss of a sample with temperature is very important because it can give us information about purity of the sample, removal of impurities from the sample and decomposition of the sample. The (TGA) thermogravimetric analysis and (DSC) differential scanning calorimetric investigation of the sample is given by figure 4(a) and figure 4(b) respectively. The curve has been divided into three regions i.e., zone 1 (20 to 230 ^0C), zone 2 (230 to 790 ^0C) and zone 3 (790 to 1000 ^0C). Initially, an

endothermic reaction has been observed in figure 4(a) which usually indicates decomposition in TGA. At a temperature of 230 ^{0}C, (3.4 %) weight loss has been observed in figure 4(a) which accounts for the removal of impurities. Sukmarani et al. [12] also observed a weight loss of (3.8 %) in their finding for a temperature range of (20 to 218 ^{0}C). The decomposition continues in the second zone in figure 2(a) in which a weight loss of (7.9%) occurred. An exothermic reaction has been observed in zone 3 at 760 ^{0}C given by the DSC curve in figure 2(b) and as a result a small weight gain has been observed in TGA analysis figure 2(a) in the similar zone. Martins et.al. [26] found that the weight gain occur because of the creation of a novel crystalline phase. Hence, the weight gain in our sample in zone 3 accounts for the creation of a new phase i.e., Mn-ferrite. In XRD analysis, we found that the phase formation of manganese ferrite starts at 1000 ^{0}C and TGA analysis also successfully reported the formation of crystalline phase at 1000 ^{0}C.

3.4. Scanning electron microscopy (SEM) analysis

Morphology of the created nano-particles is analyzed by scanning electron microscope (SEM) figure (5). The small crystallites fig (5a) are embedded in silicate layer. This layer is formed by the silica present initially as an impurity in Mn-ore which, after heat treatment, is melted and form silicate layer [27]. These embedded particles within silicate layers account for the strength of the synthesized sample. The presence of silica is also reported by XRD analysis figure (2) hence, SEM confirmed XRD analysis. The surface around these crystallites contain small pores figure (a) which arises due to the exhaust of gases during heat treatment process. Salar et.al. [27] also found similar results hence, the present results are matched with previously reported experimental results.

The platelet like structures figure (5b) belong to traces of ferric oxide (Fe_2O_3) which were initially mixed with Mn-ore during sample preparation. Similar platelet like structures were also reported by Mollamahaleh et.al. [28]. The platelet like structures were also confirmed by tunneling electron microscopy (TEM) figure (7b) are further explained TEM analysis. Literature suggests that these platelet-like structures figure (5b), indicating traces of Fe_2O_3, accounts for best magnetic properties and high melting point of the synthesized manganese ferrite nanoparticles [29].

3.5. Energy dispersive X-ray (EDX) analysis

In figure 5a, most of the particles are dark while few of them are bright which may be due to the existence of different elemental composition in the synthesized nanoparticles. In order to know in detail about the elemental distribution of the sample, (EDX) energy dispersive x-ray spectroscopy of the sample was performed figure 6. EDX spectra of the selected region A in figure 5a is given by fig 6a which represent the existence of O, Fe, Si and Mn in different weight percent depicted in table 2. The presence of Si and O in fig 6a further confirm the formation of silicate layer which was also detected in SEM micro image of figure 5a. Hence, EDX spectra confirm the SEM analysis. Salar et.al. [27] also found similar elemental composition for Mn-ferrite nanoparticles.

EDX spectra of the selected region B in figure 5b is shown in figure 6b. This spectra confirm the presence of O, Mn and Fe in different weight percent given by table 2. The high concentration of Fe, which is 53.7% by weight given by table 2, and the presence of oxygen in the selected region B of figure 5b indicate the formation Fe_2O_3 which further confirm SEM analysis of figure 5b in which the platelet structures were considered as traces of Fe_2O_3.

Table 2

Weight percent of different elements detected via EDX for region A and B of figure 5a and 5b respectively.

Figure	Micro region	Element (weight%)			
		O	Fe	Si	Mn
5a	A	12.3	49.9	2.3	35.06
5b	B	9.3	53.7	____	36.9

3.6. Tunneling electron microscopic (TEM) and selected area electron diffraction (SAED) analysis

To find size, shape, and polydispersity of the prepared samples, tunneling electron microscopy (TEM) analysis was performed (figure 7). Most of the particles in fig 7a are of regular and spherical shape which might be due to the nature of metal precursors present in the low-grade manganese ore. Regular shape of the nanoparticles is an indication of improved crystallinity which arises due to a highly synchronous nucleation and growth at well-defined temperatures. The mean size of these particles is in line with the one predicted by XRD. The variation in size of some of the nanoparticles is shown by the histogram in fig 7a is because of the surfactants present in manganese ore which reduces the surface tension and promotes spreading properties. Polydispersity of the sample was determined via equation (iv). A slight polydispersity is noted for the sample as predicted by the curve of fig 7a which arises because of the size distribution of the synthesized Mn-ferrite nano-particles.

The polydispersity index calculated from equation (4) is 0.5 which show that the material is monodisperse. This depicts that the obtained samples will show homogeneity in various conducting properties like electric properties and magnetic properties.

Scanning electron microscope (SEM) images Fig 5 having plate chip like structures are also confirmed by TEM analysis figure 7b. high resolution TEM image fig 7c of the chip like structures shows that these platelet chips consist of nano rods having a thickness of about 10.2μm. These rods are uniform and having no porosity which accounts for the strength of the obtained samples and confirms the homogeneity. The (SAED) selected area electron diffraction arrangement fig 7d confirm the crystallinity of the material and show that it is a polycrystalline material. Figure 7 d also show the diffraction patterns of (1 1 1), (2 0 0), (2 2 0), (3 1 1) and (2 2 2) planes respectively for the synthesized manganese ferrite samples which confirms the formation of manganese ferrite nano particles. Similar planes were also reported in X-ray analysis (figure 3). The measured lattice spacing was 2.95 , 2.05 , 1.56 , 1.42 and 1.28 Å for (1 1 1), (2 0 0), (2 2 0), (3 1 1) and (2 2 2) planes respectively.

$$PDI = M_w / M_n \quad (4)$$

Where PDI is the dispersity, M_w represent the weight average molecular weight and M_n is the number average molecular weight.

4. Conclusion

The pyrometallurgical method has successfully synthesized manganese ferrite nanoparticles at sintering temperatures of 1000, 1100 and 1200 ^{0}C from ferric oxide (Fe_2O_3) and low-grade manganese ore powder with highest peak intensity at sintering temperature of 1200 ^{0}C. X-ray analysis confirmed the phase formation of manganese ferrite nanoparticles. An increase in particle size and decrease in variation of lattice parameters for the synthesized nanoparticles has been reported. It is found that the edge dislocation density and micro strain of the prepared manganese ferrite nano-particles decreases with rising sintering temperature. The characteristic peaks of ferrites were also confirmed by FTIR patterns. An exothermic reaction has been observed at 760 ^{0}C indicating the formation of manganese ferrite. It is found that the thermal decomposition of the samples begin at 100 ^{0}C. it has been established that the synthesized nanoparticles possess a porous surface morphology, higher strength, best magnetic properties, high melting point, and homogeneity in conducting properties. Moreover, it is found that different characterization techniques have good coordination for the synthesized manganese ferrite nanoparticles.

Declarations

Data availability Statement:

All the data is given within the manuscript.

References

1. Junaid, M., et al., *Structural elucidation and dielectric behavior evaluation of Dy–Ni substituted manganese ferrites.* 2021. **602**: p. 412494.
2. Mathew, D.S. and R.-S.J.C.e.j. Juang, *An overview of the structure and magnetism of spinel ferrite nanoparticles and their synthesis in microemulsions.* 2007. **129**(1-3): p. 51-65.
3. Kim, Y.I., D. Kim, and C.S.J.P.B.C.M. Lee, *Synthesis and characterization of CoFe2O4 magnetic nanoparticles prepared by temperature-controlled coprecipitation method.* 2003. **337**(1-4): p. 42-51.
4. Kim, D., et al., *Synthesis and characterization of surfactant-coated superparamagnetic monodispersed iron oxide nanoparticles.* 2001. **225**(1-2): p. 30-36.
5. Gorter, E.W.J.P.R.R., *Saturation magnetization and crystal chemistry of ferrimagnetic oxides. I. II. Theory of ferrimagnetism.* 1954. **9**: p. 295-320,321-365.

6. Ahmed, Y.J.C.I., *Synthesis of manganese ferrite from non-standard raw materials using ceramic technique.* 2010. **36**(3): p. 969-977.
7. Burojeanu, V.M., et al., *Cation distribution and magnetic properties of manganese ferrite powder prepared by coprecipitation from MnO2 and FeSO4· 7H2O.* 2001. **3**(6): p. 525-529.
8. Burojeanu, V.M., et al., *Cation distribution and magnetic properties of manganese ferrite powder prepared by coprecipitation from MnO2 and FeSO4· 7H2O.* 2001. **3**(6): p. 525-529.
9. Gajbhiye, N. and G.J.T.A. Balaji, *Synthesis, reactivity, and cations inversion studies of nanocrystalline MnFe2O4 particles.* 2002. **385**(1-2): p. 143-151.
10. Misra, R., et al., *A comparison of the magnetic characteristics of nanocrystalline nickel, zinc, and manganese ferrites synthesized by reverse micelle technique.* 2004. **111**(2-3): p. 164-174.
11. Li, Y., et al., *X-ray diffraction and Mössbauer studies of phase transformation in manganese ferrite prepared by combustion synthesis method.* 2004. **87**(1): p. 91-95.
12. Sukmarani, G., et al., *Synthesis of manganese ferrite from manganese ore prepared by mechanical milling and its application as an inorganic heat-resistant pigment.* 2020. **9**(4): p. 8497-8506.
13. Naseri, M.G., et al., *Synthesis and characterization of manganese ferrite nanoparticles by thermal treatment method.* 2011. **323**(13): p. 1745-1749.
14. Yang, H., et al., *Water-soluble superparamagnetic manganese ferrite nanoparticles for magnetic resonance imaging.* 2010. **31**(13): p. 3667-3673.
15. Pande, S., et al., *Single-Step Synthesis of Manganese Ferrite Nanoparticles with Enhanced Magnetization via Chemical Co-precipitation Route.* 2019. **11**(2): p. 225-234.
16. Kafshgari, L.A., et al., *Synthesis and characterization of manganese ferrite nanostructure by co-precipitation, sol-gel, and hydrothermal methods.* 2018.
17. Zhang, B., et al., *Synthesis of magnetic manganese ferrite.* 2007. **22**(3): p. 514-517.
18. Hylander, L.D., R.B.J.E.s. Herbert, and technology, *Global emission and production of mercury during the pyrometallurgical extraction of nonferrous sulfide ores.* 2008. **42**(16): p. 5971-5977.
19. Issa, B., et al., *Magnetic nanoparticles: surface effects and properties related to biomedicine applications.* 2013. **14**(11): p. 21266-21305.
20. Gonçalves, N., et al., *Size–strain study of NiO nanoparticles by X-ray powder diffraction line broadening.* 2012. **72**: p. 36-38.
21. Andrade, A.B., N.S. Ferreira, and M.E.J.R.a. Valerio, *Particle size effects on structural and optical properties of BaF 2 nanoparticles.* 2017. **7**(43): p. 26839-26848.
22. Hua, T.I., R.J.M.J.o.F. Sundari, and A. Sciences, *Fabrication and characterization of ferrites (Mg and Mn) based on FTIR, XRD, SEM and TEM.* 2012. **8**(3).
23. Shanmugavel, T., et al., *Synthesis and structural analysis of nanocrystalline MnFe2O4.* 2014. **54**: p. 159-163.
24. Islam, K., et al., *Manganese ferrite nanoparticles (MnFe2O4): Size dependence for hyperthermia and negative/positive contrast enhancement in MRI.* 2020. **10**(11): p. 2297.

25. Zipare, K., et al., *Superparamagnetic manganese ferrite nanoparticles: synthesis and magnetic properties.* 2015. **1**(3): p. 178-182.
26. Martins, M.L., et al., *Mechanisms of phase formation along the synthesis of Mn–Zn ferrites by the polymeric precursor method.* 2014. **40**(10): p. 16023-16031.
27. Ahmad, S., et al., *Synthesis and characterization of manganese ferrite from low grade manganese ore through solid state reaction route.* 2021. **11**(1): p. 1-9.
28. Mollamahaleh, Y.B., et al., *Surfactant-free production of Ni-based nanostructures.* 2011. **2**(05): p. 444.
29. Harizanova, R., et al., *EBSD investigation and magnetic properties of manganese ferrite crystallized in a sodium-silicate glass.* 2018. **20**(30): p. 4268-4276.

Figures

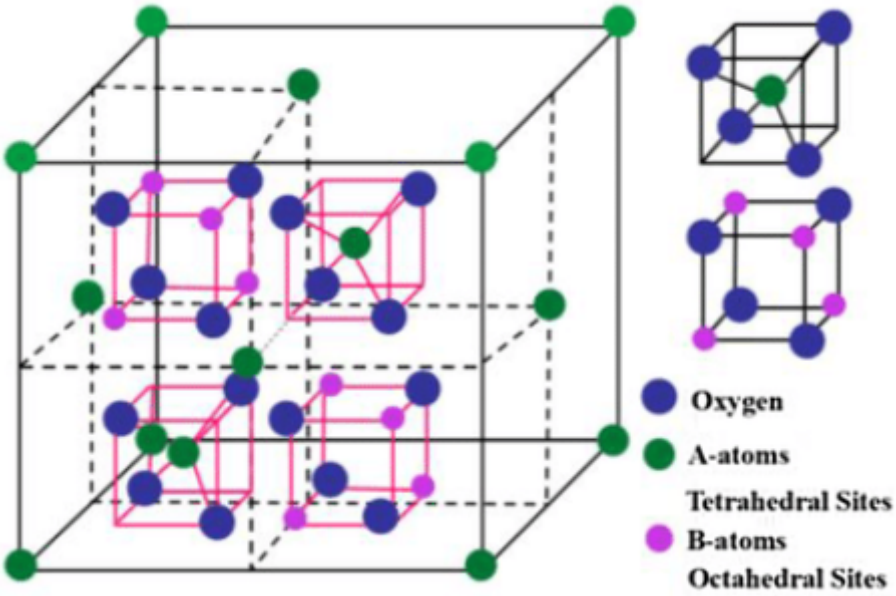

Figure 1

Spinel lattice cell with octahedral and tetrahedral frameworks [19]

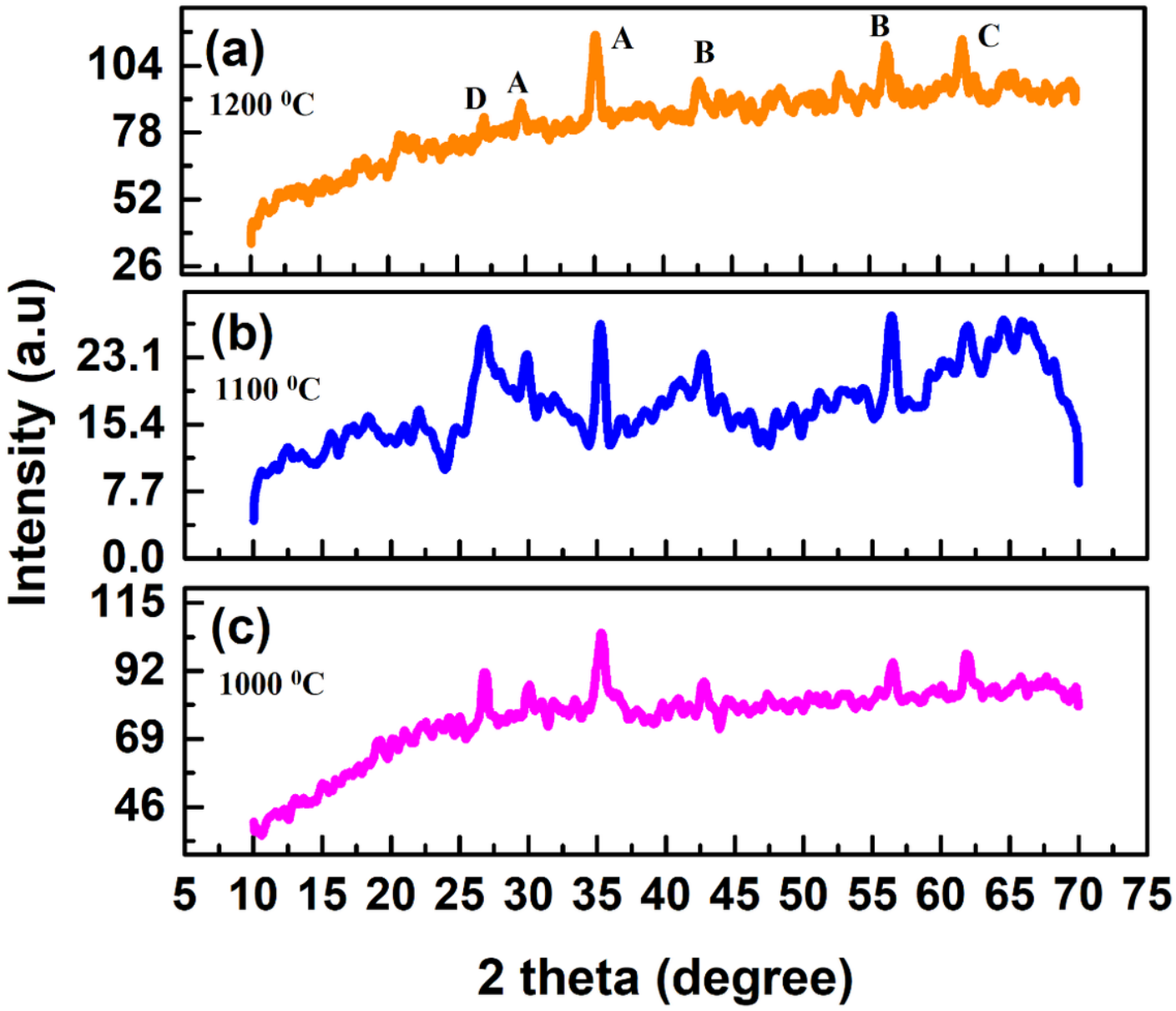

Figure 2

X-ray analysis of the samples sintered at different temperatures with labelled peaks

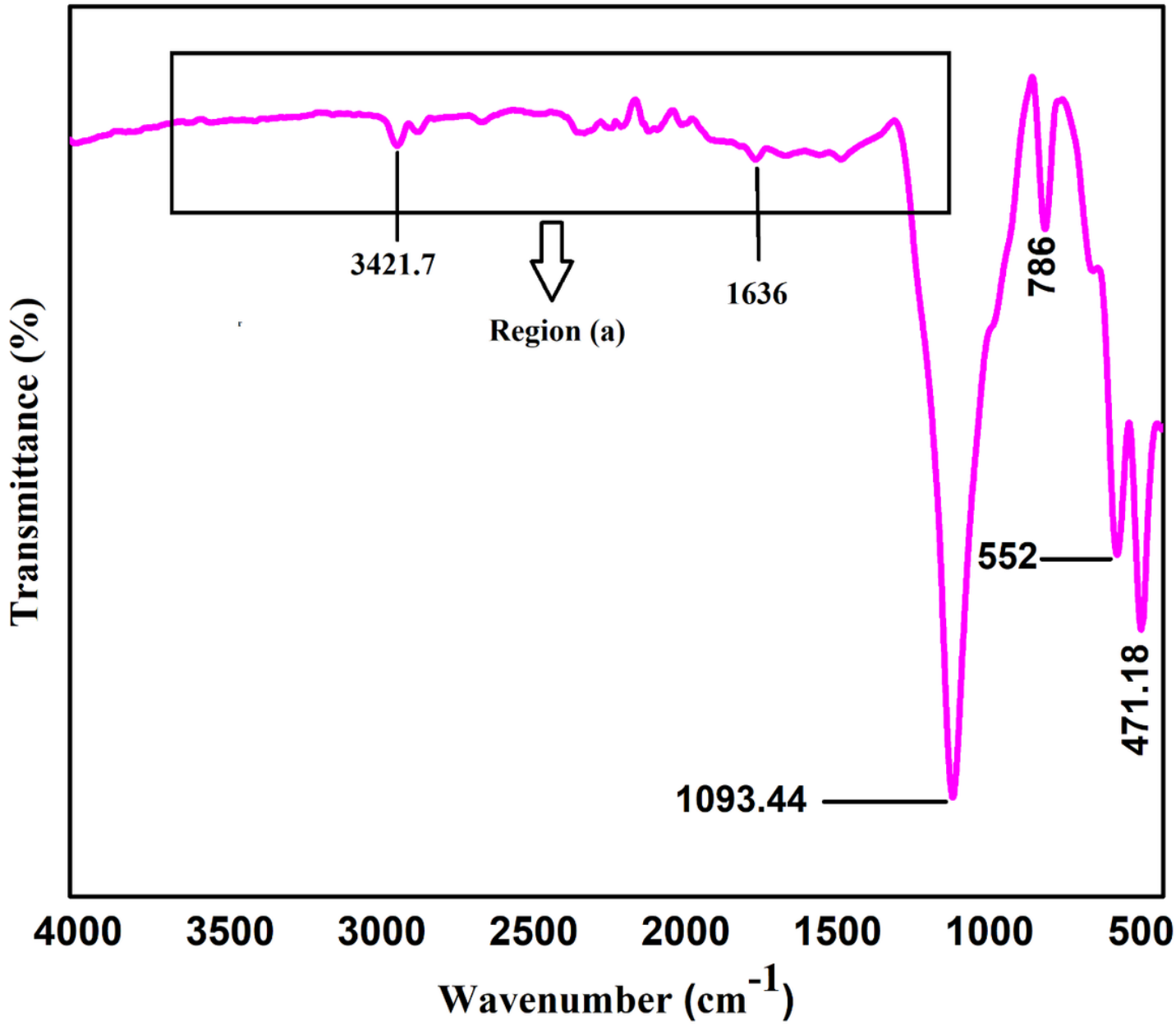

Figure 3

FTIR spectra of manganese ferrite nanoparticles

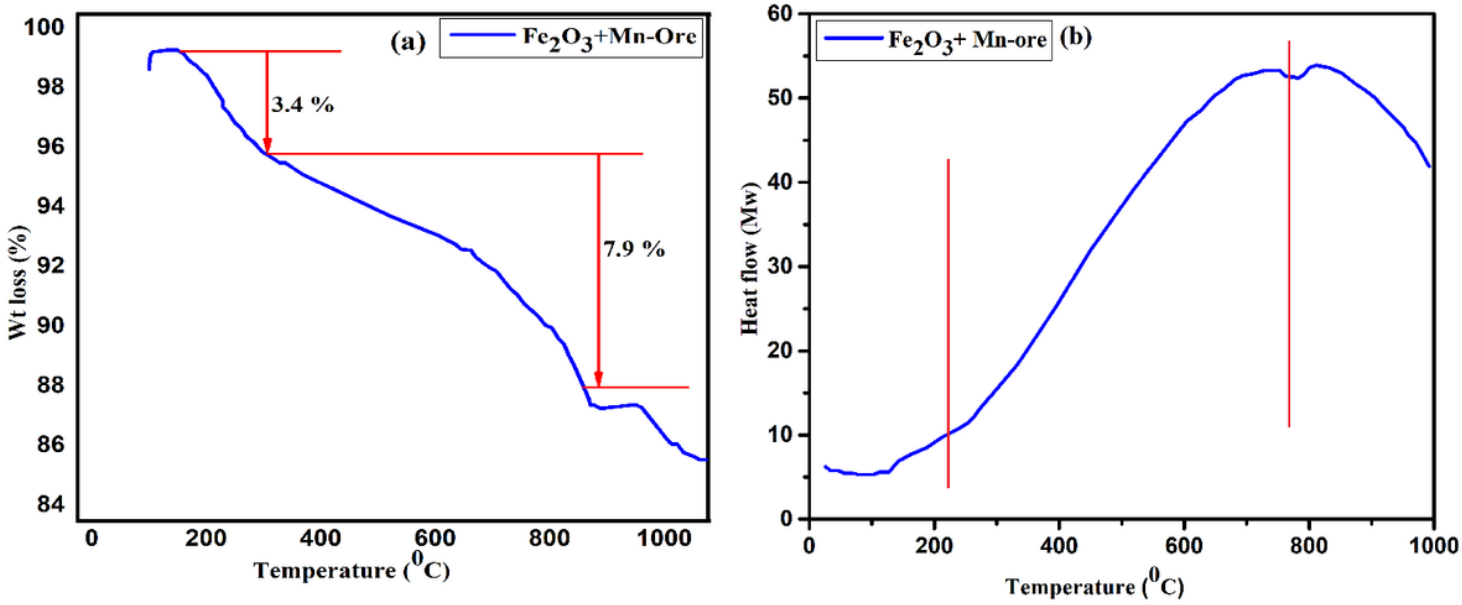

Figure 4

(a) Thermogravimetric analysis (TGA) curve (b) Differential scattering calorimetry (DSC) curve

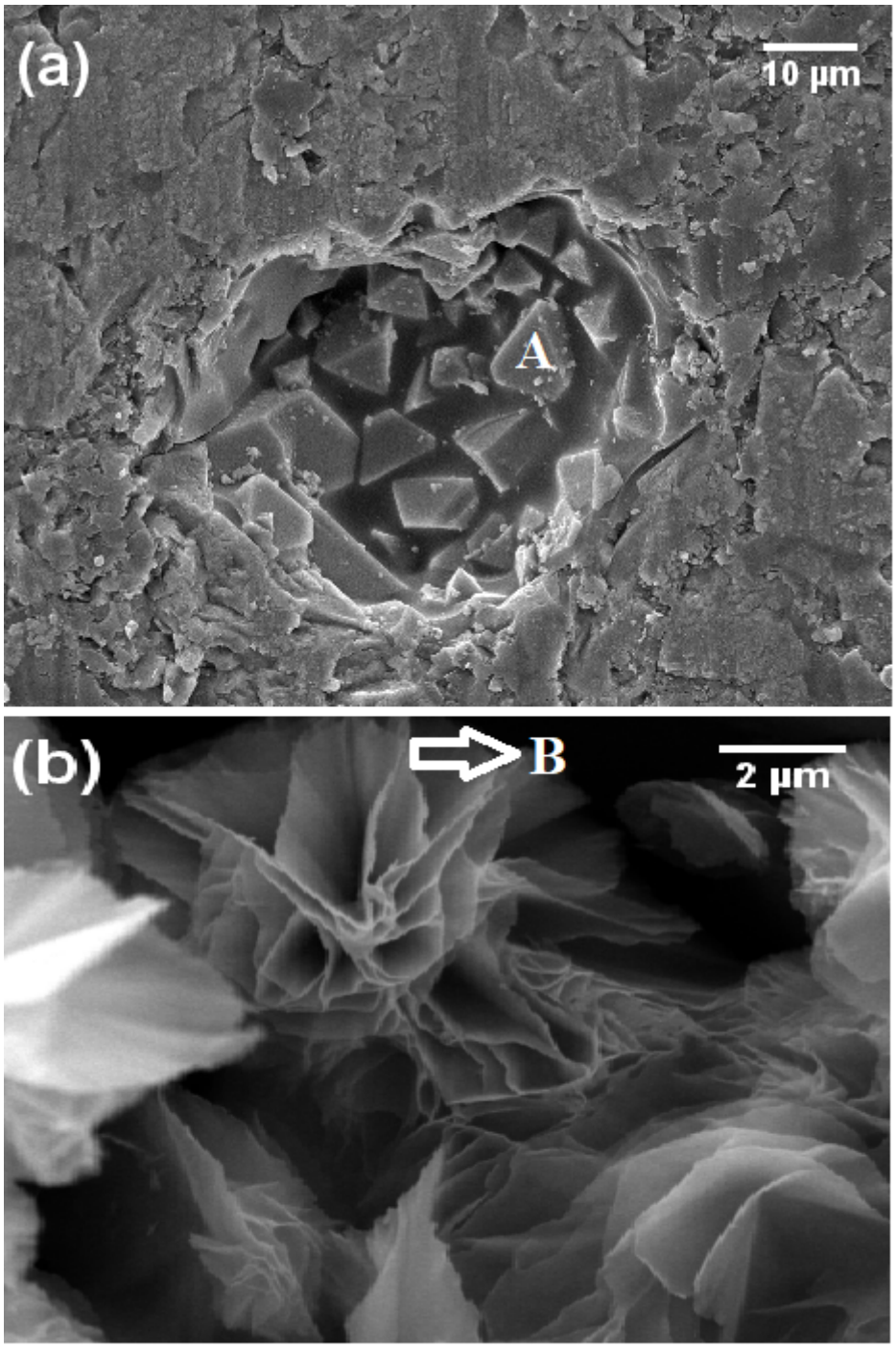

Figure 5

Scanning electron microscope (SEM) images of Mn-ferrite nanoparticles

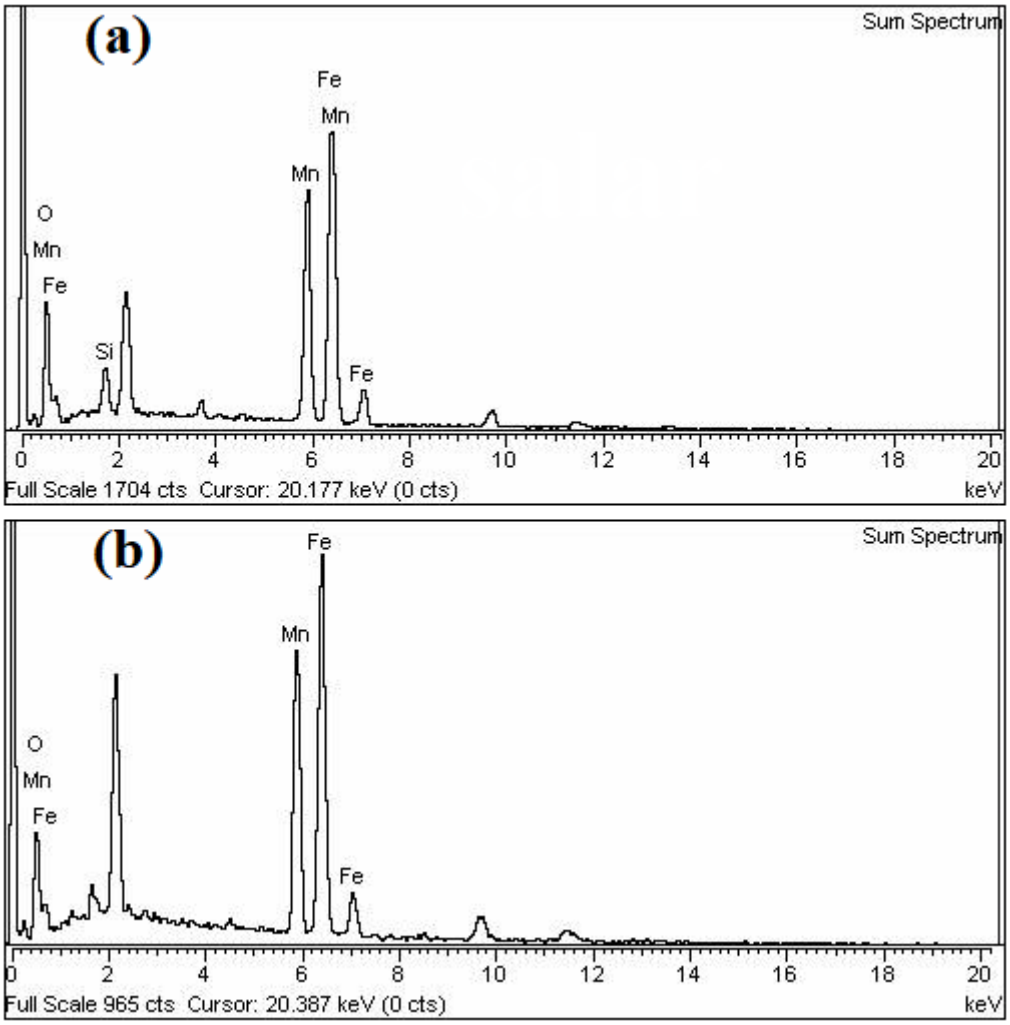

Figure 6

(a) Show EDX spectra of indicated region A in figure 5a and (b) EDX spectra of indicated region B in figure 5b.

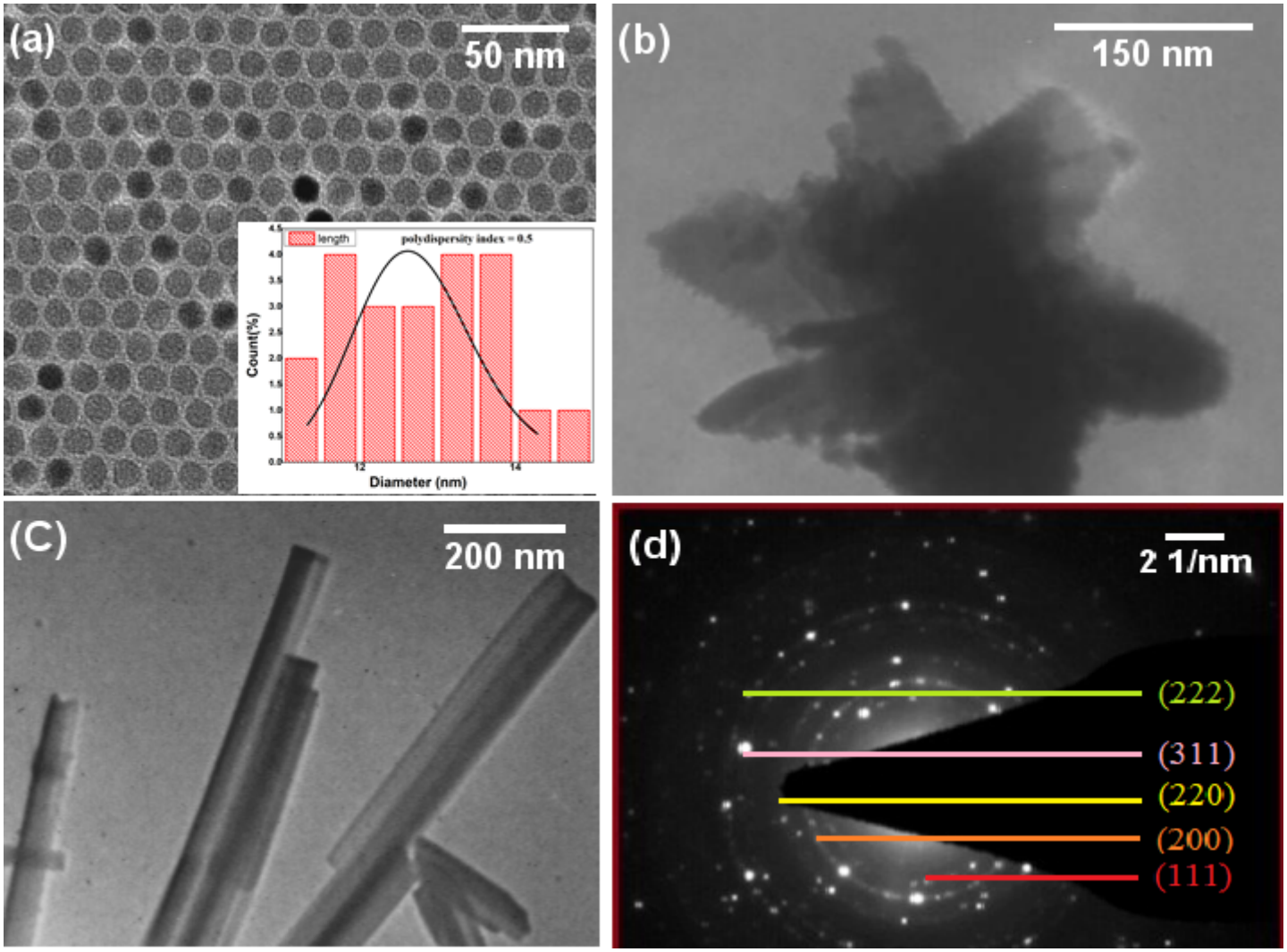

Figure 7

TEM images (a-c) and SAED micrographs (d) of manganese ferrite nano particles

Supplementary Files

This is a list of supplementary files associated with this preprint. Click to download.

- floatimage1.png